Physics of Plasmas ARTICLE scitation.org/journal/php

Supersonic water jets as point-like sources of extremely high pressure

Cite as: Phys. Plasmas **30**, 022710 (2023); doi: 10.1063/5.0135486
Submitted: 20 November 2022 · Accepted: 25 January 2023 ·
Published Online: 21 February 2023

D. Maler,[1,a)] R. Grikshtas,[1] S. Efimov,[1] L. Merzlikin,[1] M. Liverts,[2] M. Kozlov,[3] and Ya. E. Krasik[1]

AFFILIATIONS

[1]Physics Department, Technion-Israeli Institute of Technology, Haifa 3200003, Israel
[2]Engineering Mechanics Department, Royal Institute of Technology, Stockholm 114 28, Sweden
[3]Center for Preparatory Studies, Nazarbayev University, Nur-Sultan 010000, Kazakhstan

[a)]**Author to whom correspondence should be addressed:** daniel.maler@campus.technion.ac.il

ABSTRACT

Two interacting supersonic water jets and collisions of a water jet with an aluminum target are studied experimentally and by hydrodynamic simulations. Supersonic water jets form, when shocks generated by underwater electrical explosions of conical wire arrays converge. The arrays are supplied by a ∼250 kA, ∼1 μs rise time current pulse. Underwater explosion of two conical arrays placed face to face produces jets propagating in air with velocities of $\sim 2.5 \times 10^3$ m/s leading to hot plasma formation at a temperature of ∼2200–3000 K, pressure $\sim 1.7 \times 10^{10}$ Pa, and density $>10^{29}$ m^{-3}. When a single array explodes underwater in front of an aluminum target, the collision of the jet with the target produces a local pressure of $\sim 3 \times 10^{10}$ Pa on the surface of the target.

I. INTRODUCTION

Recent studies[1–5] of underwater electrical wire explosions (UEWE) of a single wire and wire array using μs- and sub-μs timescale high-current generators (stored energy of several kJ) demonstrated the applicability of this approach for research related to Warm Dense Matter (WDM) and High Energy Density Physics[6–10] (HEDP). An UEWE is accompanied by rapid solid–liquid–vapor-plasma phase transitions with energy density deposition of several tens of MJ/kg. During the vapor–plasma phase transition, the wire temperature and pressure reach several eV and $\sim 10^{10}$ Pa. This phase transition is accompanied by fast radial wire expansion which leads to a rather efficient (≥24%) transfer of the deposited energy into the wire to the water shock and the waterflow behind the shock front.[11,12] In addition, for explosions of cylindrical or spherical wire array geometries, the converging shocks can produce extremely high pressures ($\geq 10^{11}$ Pa), densities ($\geq 2 \times 10^3$ kg/m^3), and temperatures (≥2 eV) at the vicinity of the shock implosion.[5,13]

In our recent experiments,[14–16] it was shown that μs- and sub-μs timescale UEWE of either cylindrical or conical wire arrays can generate supersonic sub-millimeter diameter water jets at velocities reaching up to $\sim 5 \times 10^3$ m/s. It was demonstrated that the velocity of the jet in air depends on the array geometry and the water layer's thickness above the edge of the array. Also, it was found that a higher energy density deposition rate into the wires results in faster radial wire expansion and a stronger converging shock, leading to higher jet velocities. In Ref. 16, the generation of high velocity water jets was studied using FLASH simulations where the converging shockwaves produced by the explosion of wires in water were recreated to match the experimental results. It was shown that the generation of water jets is the result of two combined effects. The first effect is the strong shock and the waterflow behind the shock front generated by the explosion of cylindrical/conical wire array. Convergence of this shock and the waterflow to the symmetry axis results in extreme parameters of the water with pressure, water density, and waterflow velocity exceeding 3×10^{10} Pa, 2×10^3 kg/m^3, and 3×10^3 m/s, respectively. The second effect is related to the edge effect at the array's edge where the shock propagates in a funnel shape, realizing a cumulation effect along the non-simultaneous convergence of the funnel-shaped shock. Thus, together with the extreme water parameters along the symmetry axis, inducing a high-pressure gradient toward the array edge, a high velocity water jet is formed. This earlier research suggested that such supersonic jets can be used in HEDP studies, research on hydrodynamic instabilities, and possibly the exploration of the low energy D–D reaction cross section. For instance, interaction of supersonic water

microjets can be considered as an attractive approach to study interacting particle flows similarly to the studies of the plasma jets generated by the powerful OMEGA EP laser pulse's interaction with tin targets.[17]

In the present paper, we describe the results of two sets of experiments as follows: (a) the interaction of counterstreaming jets generated by the explosions of two conical arrays placed face to face and (b) the interaction of supersonic jets with an aluminum target. The results show that in both configurations, the generated supersonic water jets can be used in the research of extreme states of matter.

II. EXPERIMENTAL SETUP AND DIAGNOSTICS

The experimental setup [see Fig. 1(a)], used in the present research, is similar to that described in Ref. 15. Experiments were carried out using a μs-timescale generator[18] with $C = 10$ μF, 30 kV charging voltage, ~250 kA current amplitude, and ~1.1 μs rise time on a short circuit load with an inductance similar to that of the load. The waveforms of the discharge current (I) and voltage (V) along the load were measured using a calibrated self-integrated Rogowski coil (measurement error of ±5%) and a Tektronix P6015A high-voltage (HV) divider (measurement error of ±3%). The inductive voltage LdI/dt was subtracted from the measured value of V to obtain the resistive voltage V_r, where L is the inductance of the array determined in short-circuit shots with non-exploding loads imitating the array.

In experiments with counterstreaming jets [see Fig. 1(b)], two 40 mm long, truncated cone arrays, consisting of 27 copper wires, 100 μm diameter each, generated supersonic water jets. Each array with an apex angle of 3.57° has an HV and ground electrodes with 10 and 5 mm diameter holes, respectively. The wires were soldered to the external surfaces of the electrodes. The arrays were placed coaxially face-to-face in a stainless-steel chamber filled with de-ionized water, and optical observations were made through a Perspex window. A 6 mm thick dielectric capsule was placed on the axis between the HV electrodes. The capsule was separated from the array HV electrodes by two 1 mm thick aluminum diaphragms with 3 mm diameter holes. These diaphragms were used to decrease the intensity of the light emission of the exploded wires. The capsule has two 4 mm diameter optical windows located opposite each other and an input hole for a 1 mm diameter optical fiber [see "fiber holder" in Fig. 1(b)]. The fiber, placed inside the hole, was collimated so that it collects light emission from an air volume of ~1.5 mm diameter at the center of the dielectric capsule. The fiber was connected to an R7400U-04 photo-multiplier tube (PMT), registering the temporal evolution of the emitted jet light.

At the HV end of the array, each capsule was sealed by a 10 μm thick aluminum foil which separates an air–water interface. Thus, jets, generated by conical wire array electrical explosions, propagated through a 2 mm thick water layer, punched through the foils and interacted inside an air-filled volume of the capsule. To study this interaction, a continuous wave (CW) single mode laser (1.5 W, 532 nm) was used to produce shadow images of the jets propagating in air which were recorded using an XXRapidFrame ICCD multi-channel framing camera (Stanford Computer Optics Inc.). In other

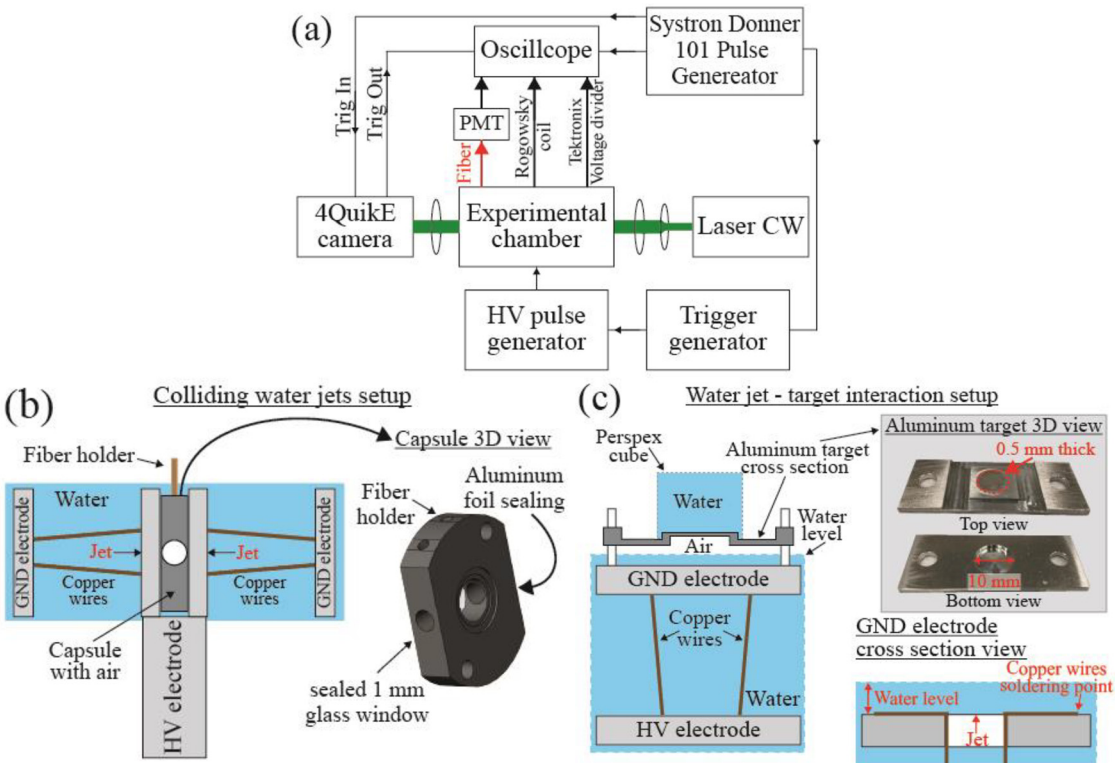

FIG. 1. (a) Experimental setup and diagnostics; (b) sketch of the two face-to-face wire arrays with a hermetically sealed capsule placed between them; and (c) sketch of the setup of the water jet's interaction with an aluminum target placed above the water and the target itself.

experiments, we used the XXRapidFrame ICCD camera to obtain an image sequence of light emitted by the jets inside the capsule prior and after the interaction.

Research of water jets colliding with an aluminum target [see Fig. 1(c)] was performed using electrical explosions of a truncated 40 mm long, the same as in two cones array but with 40 copper wires of 114 μm diameter. The array was placed in the same experimental chamber, fully submerged in de-ionized water. Above the array, a 0.5 mm thick target was placed ∼3 mm above the water surface. In these experiments, the water layer thickness above the 10 mm diameter grounded electrode was ∼2 mm. A sealed rectangular Perspex cube, transparent for visible light and filled with water, was placed on the upper surface of the target [see "Perspex cube" in Fig. 1(c)]. Interaction of the jet with the target leads to the formation of a shock which, upon reaching the target's upper boundary, generates a shock in the water contained in this cube. In these experiments, the grounded electrode, water, air, and the capsule were backlit by a CW single mode laser (532 nm), to produce shadow images of the water jet propagation in air and the shock in the cube water. These shadow images were recorded using the XXRapidFrame ICCD camera. By producing a sequence of images, with known time interval between frames, we calculate the jet and shock velocity. Due to the smearing of the jet and shock fronts, the error in the jet and shock velocity measurement δv was calculated to be $\pm$150 m/s. In several experiments, laser backlighting was not used and framing images of the jet's light emission were registered. Additionally, we applied a Photonic Doppler Velocimetry (PDV) (see Ref. 18) to measure the velocity of the target acquired due to the interaction with the water jet and that of the subsequent waterflow.

The waveforms of the discharge current, voltage, PMT, and output synchronization pulses of the framing camera were acquired using a Tektronix TDS5104B digitizing oscilloscope. For the synchronization of the pulse generator's operation with the framing camera, a Systron Donner 101 Pulse Generator was used.

III. EXPERIMENTAL RESULTS

A. Interaction of two counterstreaming jets

Typical waveforms of the discharge current, resistive voltage, deposited power, and energy obtained in these experiments are shown in Fig. 2. One can see that the wire arrays explosion is characterized by an almost critically damped discharge where ∼75% of the energy stored in the pulse generator was deposited into the wires during ∼500 ns.

Shadow images of jets, obtained at different times, while propagating toward each other in air inside the capsule, are shown in Fig. 3. One can see that two counterstreaming jets approach each other [see Figs. 3(a)–3(b)] forming eventually a water column [see Fig. 3(d)]. Using time-of-flight data, the velocity of each jet was estimated to be $(2.45 \pm 0.15) \times 10^3$ m/s. Let us note that in Fig. 3, the jets have slightly different radii (∼0.17 and ∼0.2 mm) and slightly non-coaxial coinciding trajectories. It is difficult to align these counter collisions. In some explosion experiments, the jet trajectories did not even overlap. Nevertheless, the data obtained here are sufficient to make a rough estimate of the possible pressures and temperatures when these jets do interact with each other.

In Fig. 4, we present images of the light emitted by the jets propagating in air inside the capsule at two different times. To obtain this light emission, the frame duration was increased from 10 to 35 ns and the camera amplification from 820 to 990 V resulting in an increase by a factor of ∼28 of the camera sensitivity compared to shadow imaging experiments. In Fig. 4(a), one can see two ∼0.5 mm diameter light sources which can be associated with the jets propagating in air which become approximately a single light source near the center of the capsule at 5.8 μs [Fig. 4(b)].

In Fig. 5, typical waveforms of the discharge current, resistive voltage together with the framing camera synchronization pulses and the light registered by the PMT are shown. The PMT signal has two peaks corresponding to light emission. The first peak occurs long before the appearance of frame (a) in Fig. 4, while the second peak coincides with the jets collision in Fig. 4(b). Therefore, the first peak may be the result of the implosion of the strong shock at the axis of each cone which is accompanied by a strong light emission.[19–21] The later peak of light emission can be considered to correspond to the time when the jets enter the capsule and interact with each other.

B. Interaction of a jet with an aluminum target

In this set of experiments, the electrical explosion of a single conical wire array is characterized by discharge current and voltage waveforms similar to those shown in Fig. 2. First, we used a PDV to measure the velocity acquired by the target due to the interaction with the water jet which is followed by a waterflow. These measurements showed that target velocity can reach ∼300 m/s due to acceleration by

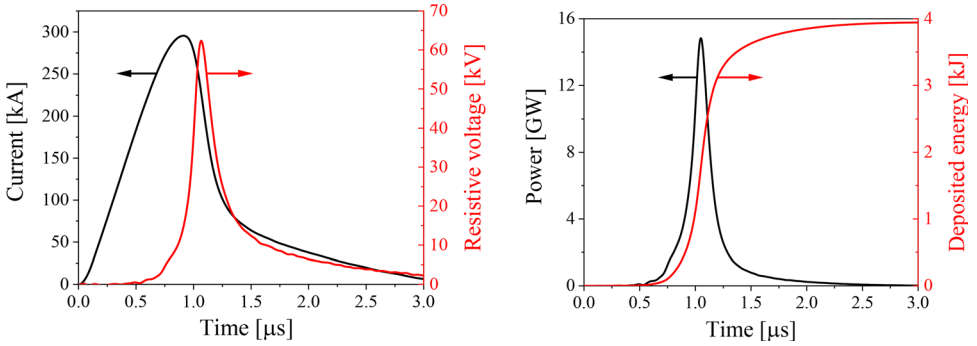

FIG. 2. Typical waveforms of the discharge current and resistive voltage (left) and deposited power and energy (right).

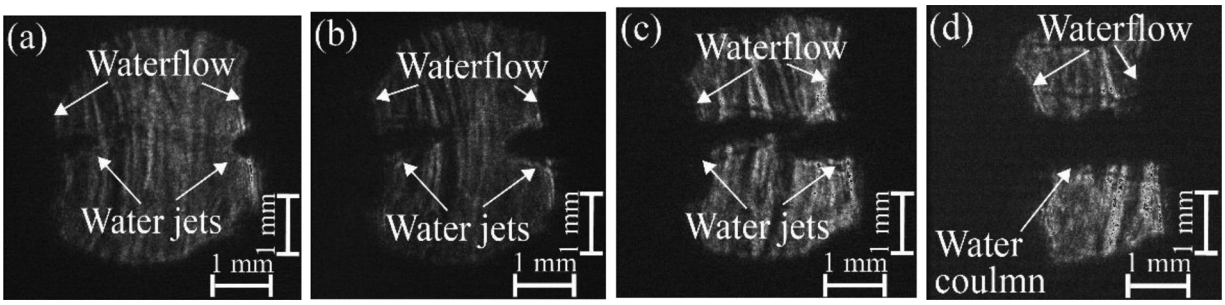

FIG. 3. Shadow images of jets propagating toward each other in air inside the capsule. (a) $t = 4.2$, (b) $t = 4.5$, (c) $t = 4.8$, and (d) $t = 5.2$ μs. The frame duration is 10 ns. $t = 0$ is defined at the beginning of the discharge current.

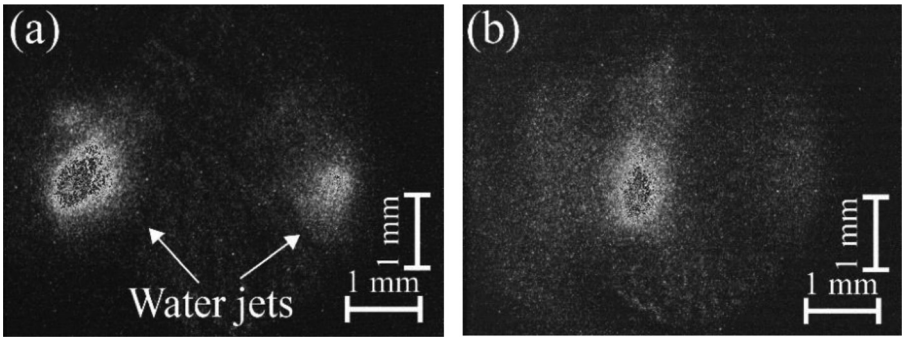

FIG. 4. Self-emission images of jets propagating toward each other in air inside the capsule. (a) $t = 4.8$ and (b) $t = 5.8$ μs. Frame duration is of 35 ns. $t = 0$ is the beginning of the discharge current.

the axial waterflow which follows the jet. However, because of the jet's submillimeter size, we could not separate the contribution of the interaction with the jet from that of the waterflow to the velocity of the target's upper surface.

We first applied shadow imaging to obtain the jet velocity shown in Fig. 6. Using time-of-flight data, the jet velocity was determined as $v_j \cong (2.8 \pm 0.15) \times 10^3$ m/s which decreased to $v_j \cong (2.3 \pm 0.15) \times 10^3$ m/s at the distance where the target is placed. The velocity of the water's axial flow was determined as $v_f \sim 10^3$ m/s.

Next, we obtained light self-emission of the jet during its propagation in air and interaction with the target. In this set of experiments, the amplification of the framing camera was set to 990 V and the frame duration was increased up to 200 ns. In Fig. 7, one can see that the interaction of the jet with the target placed at a distance of 3 mm above the water level is accompanied by a mushroom like formation in the target's vicinity. Visual inspection of the target showed a ~1 mm diameter melting pattern with a 0.2 mm diameter, ~0.7 mm deep hole.

The recorded light emission from the jet allows rough estimates of the jet surface temperature assuming Planckian radiation, namely, we compared the jet's light intensity with the intensity of the backlighting laser and we found that they are the same for a laser power of ~50 μW. Next, considering the duration of the frame, the camera's photocathode's quantum efficiency for different wavelengths and the geometrical factors of the optical system, a flux density of photons was estimated by integrating the Planckian distribution in the visible range of light. In our calculation, we compared the light intensity given by a monochromatic laser, $\lambda = 532$ nm, to the intensity seen by the jet's self-emitted light. We found that a laser light (as described above) of $P_L \sim 50$ μW power yields a similar intensity on the camera as to that obtained in experiments with water jets, given the same amplification and frame duration. That is, we calculate the power density of the laser as $p_L = \frac{P_L}{S_l} = 0.16\,\mathrm{W/cm^2}$, where P_L is the laser power and S_l is the effective area of the photocathode in the camera. Next, we calculate the power density of the radiation emitted by the jet assuming Black Body (BB) radiation as

$$P_{\mathrm{BB}}\left(\mathrm{W/m^2}\right) = \int_{\Omega_1}^{\Omega_2} d\Omega \int_{\lambda_1}^{\lambda_2} B_\lambda(T)\, d\lambda. \tag{1}$$

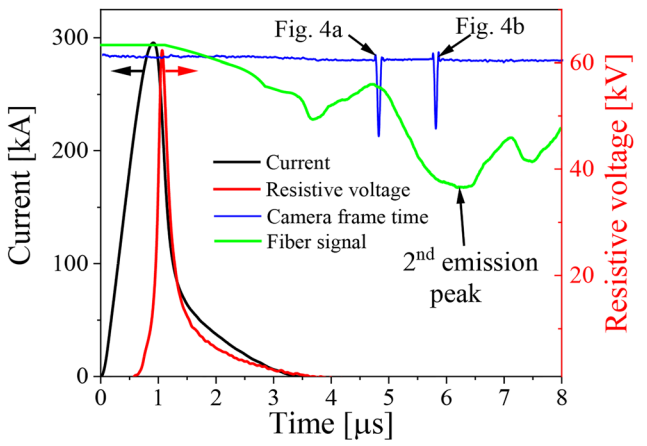

FIG. 5. Waveforms of the discharge current, resistive voltage together with the framing camera synchronization pulses, and light emission registered by the PMT.

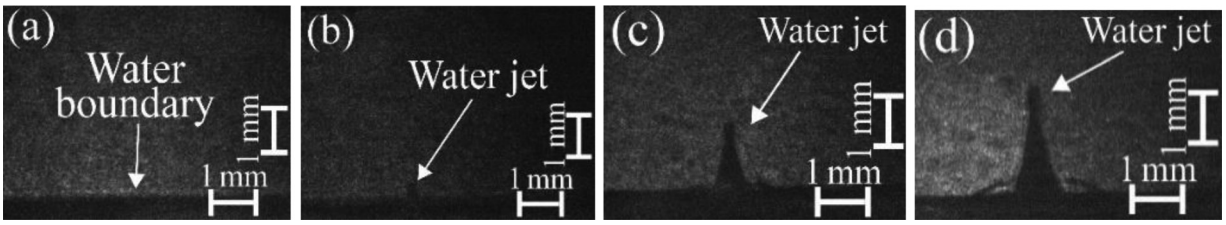

FIG. 6. Shadow images of the water jet at $t = 3.5$ (a), 4 (b), 4.5 (c), and 5 μs (d). The frame duration is 10 ns. $t = 0$ is defined as the beginning of the discharge current. Initial height of the water level is of 2 mm above the output of the conical array.

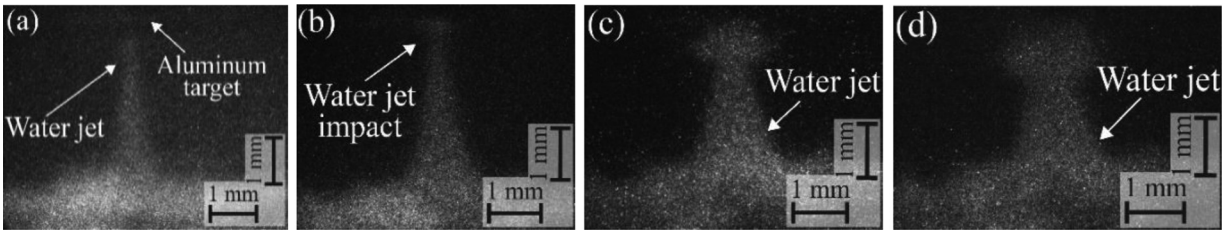

FIG. 7. Self-emission images of the water jet. (a) $t = 5.1$, (b) $t = 5.5$, (c) $t = 6.1$, and (d) $t = 6.5$ μs. The frame duration is 200 ns. Other parameters are the same as in Fig. 6.

Here, $\Omega_{1,2}$ are the solid angles determined by the optical setup used in the experiment. Considering the quantum efficiency of the camera photocathode in the range of $\lambda_1 = 350\,(\text{nm}) - \lambda_2 = 800\,(\text{nm})$, the value of P_{BB} was calculated to be equal to the value of p_L by fitting the temperature. Thus, assuming that the water jet emits light as BB radiation, the temperature of the jet surface should correspond to ~2200 K.

Finally, using the experimental setup shown in Fig. 1(c), the shock propagation in water above the aluminum target was studied. In this experiment, the water layer thickness above the output of the array was 2 mm and the distance between the water surface and target was ~3 mm. Using the shadow images of the resulting shock (Fig. 8), we calculate the average shock velocity at the distance $r_1 = 0.5$ mm from the surface of the target as $D \approx 2.2 \pm 0.15 \times 10^3$ m/s.

IV. DISCUSSION

Experimental results show that the interaction of jets generated by the underwater electrical explosion of two conical wire arrays leads to the formation of an intense light emission water state and that interaction of the single jet with an aluminum target results in a hole formation in the target and a subsequent shock in water. In order to estimate the parameters of the water and the target material during these processes, numerical simulations were carried out.

The simulations solve Euler's equation in their Lagrangian form, derived from mass, momentum, and energy conservation equations for a compressible fluid,[22,23]

$$\frac{\partial \rho}{\partial t} + \vec{\nabla} \cdot (\rho \vec{v}) = 0, \tag{2}$$

$$\frac{\partial \rho \vec{v}}{\partial t} + \vec{\nabla}(\rho \vec{v} \cdot \vec{v}) + \vec{\nabla} P = 0, \tag{3}$$

$$\frac{\partial \rho \varepsilon}{\partial t} + \vec{\nabla} \cdot \left[(\rho \varepsilon + P)\vec{v}\right] = 0, \tag{4}$$

where $\rho, \varepsilon, \vec{v}$, and P are the density, internal energy, velocity, and pressure, respectively. These equations are coupled to the SESAME EOS[24] database for Al, water, and air as $P = P(\rho, \varepsilon)$ and $T = T(\rho, \varepsilon)$. The simulation scheme used in this research was described in Refs. 22 and 23. This scheme considers division of the space into triangles with characteristic size of ~30 μm and assigns for each triangle a material with its own EOS, depending on initial conditions. At each time step, the simulation solves Eqs. (2)–(4) from which the 2D displacement of each triangle vertex, along with the density and internal energy of each triangle is calculated. Given the internal energy and density, the simulation extrapolates, using SESAME EOS tables, the pressure and temperature of each triangle.

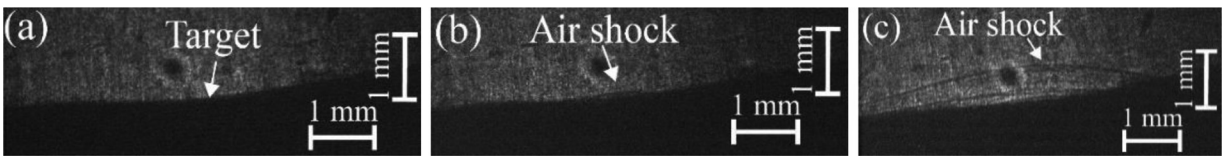

FIG. 8. Shadow images of shocks generated in water above the aluminum target. (a) $t = 5.1$, (b) $t = 5.3$, and (c) $t = 5.5$ μs. The frame duration is 10 ns. $t = 0$ is defined at the beginning of the discharge current.

The initial simulation setup for investigating the jet–target interaction is presented in Fig. 9(a). In these simulations, the initial condition of the jet velocity was 2.2×10^3 m/s, within the measured error in experiments when the jet propagated in air. As fitting parameters, we used the initial pressure, density, internal energy and temperature of the water jet in the vicinity of the bottom surface of the target to obtain a shock velocity of 2.2×10^3 m/s in water at the distance of 0.5 mm from the target upper surface. The best fit was obtained for a jet initial pressure of 10^9 Pa, a density of 1.1×10^3 kg/m^3, an internal energy of 10^6 J/kg, and a temperature of ∼1200 K. The latter is ∼1.8 times lower than the temperature estimated by BB radiation. At present, we do not know reason(s) for this disagreement. One can speculate that the higher temperature derived from the BB estimate could be related to heating of the jet due to air viscosity which was not considered in the numerical simulations. Also, it could be that the jet radiates as gray body and in this case its temperature $T_{GB} = \sqrt{a4}T_{BB}$, where $a(T) < 1$ is the gray body absorbance capacity which depends on the density of the body. Further research on the jet structure is strongly required and we are planning to use in this study radiographic images obtained at the European Synchrotron Radiation Facility (ESRF), Grenoble, France.

Figure 9(c) shows the maximal water and target parameters reached in numerical simulations for this configuration, obtained ∼1 ns after jet impact with the target. The results of these simplified simulations show that in order to obtain the best fit with experimental data, upon impact with the jet, the pressure at the target surface should reach $\sim 3 \times 10^{10}$ Pa, and the density and temperature of the target should be increased to $\sim 3.35 \times 10^3$ kg/m^3 and ∼1000 K, respectively. Additionally, after several tens of ns, the pressure and density in the water pushing against the target reached $\sim 8 \times 10^9$ Pa and $\sim 1.6 \times 10^3$ kg/m^3.

To estimate the pressure P_1 behind the shock front propagating in water, the polytropic Equation of State for water[25] $P_1 - P_0 \cong 3 \times 10^8(\delta^{7.15} - 1)$ and the Hugoniot relation for the shock velocity $D = \sqrt{\frac{(P_1 - P_0)\delta}{(\delta - 1)\rho_0}}$ are used. Here, $\delta = \rho/\rho_0$ is the compression of water and ρ_0 and ρ are the normal and compressed water densities, respectively. For a measured shock velocity of $\sim 2.2 \times 10^3$ m/s, one obtains $\delta \approx 1.2$ and $P_1 \approx 8 \times 10^8$ Pa. Now, considering that the size of the shock source is point-like with radius $r_0 \approx 0.1$ mm and that the pressure's radial distribution is $P_1 = P_{r_0}(r_0/r_1)^2$, one can estimate the energy in the half-sphere between radii r_0 and $r_1 = 1$ mm as $w = 2\pi P_0 r_0^2(r_1 - r_0) \approx 45 \times 10^{-3}$ J, which corresponds to a pressure of $\sim 1.1 \times 10^{10}$ Pa in this volume.

Simulation of colliding water jets [Fig. 9(b)] has been carried to estimate the pressure, density, and temperature at the interface where the jets collide. Here, the initial velocity for each jet was 2.5×10^3 m/s as measured in experiments to estimate the water parameters when jets collision occurs. In Fig. 9(d), we present simulation results for the maximal water parameters obtained at ∼2 ns after jets collision. The results of these simulations show that the water pressure, density, and temperature reach $\sim 1.7 \times 10^{10}$ Pa, $\sim 1.7 \times 10^3$ kg/m^3, and ∼2200 K, respectively. Here, let us note that a rough estimate of the pressure using Bernoulli's equation for an incompressible flow, considering an initial density of 1.36×10^3 kg/m^3 yields the same pressure of 1.7×10^{10} Pa.

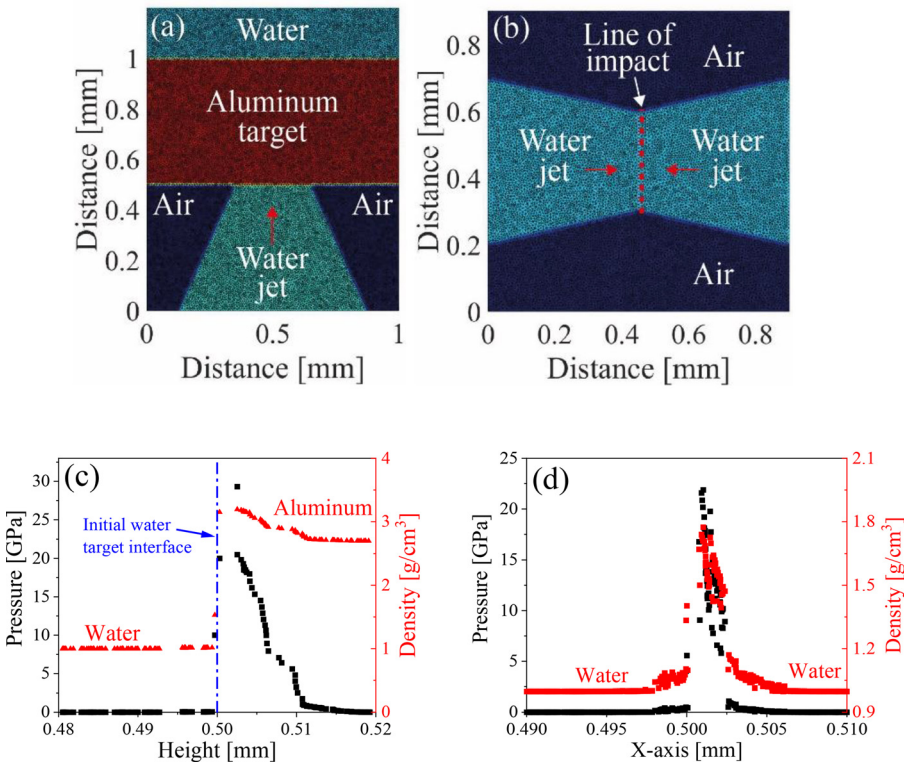

FIG. 9. Initial simulation setup for (a) water jet–aluminum target interaction and (b) jet collision. The dark blue represents normal air density, light blue—normal water density, and red—normal aluminum density. Panels (c) water jet target interaction and (d) colliding water jets show distribution of water density and pressure when maximal values of these parameters were obtained in simulations. The dashed blue line in (c) marks the initial water–target interface.

V. SUMMARY

In experiments where two counterstreaming jets collide, we find that densities and pressures reach values at which water is in an extreme state. The results of our simplified simulations show that pressures of $\sim 2.2 \times 10^{11}$ Pa, densities of $\sim 2.93 \times 10^3$ kg/m^3, and a temperature $\sim$48 700 K can be achieved in a submillimeter volume for more powerful pulse generators where the initial jet velocities can reach 10^4 m/s. These water parameters become suitable in the research of light nuclei fusion cross sections at low energies.[26,27] For the same type of generators, in situation with a single water jet interaction with an aluminum target, an initial jet velocity of 10^4 m/s yields pressures of $\sim 3.1 \times 10^{11}$ Pa, water density of $\sim 5.32 \times 10^3$ kg/m^3, and temperatures of $\sim$15 200 K. These parameters are suitable for WDM and HEDP experiments.

ACKNOWLEDGMENTS

The authors are grateful to Dr. J. Leopold for fruitful discussions. This research was supported by the Israel Science Foundation (Grant No. 418/22).

AUTHOR DECLARATIONS

Conflict of Interest

The authors have no conflicts to disclose.

Author Contributions

Daniel Maler: Conceptualization (equal); Data curation (lead); Formal analysis (lead); Methodology (equal); Software (equal); Writing – original draft (equal); Writing – review & editing (equal). **Ron Grikshtas:** Data curation (supporting); Formal analysis (supporting). **Sergey Efimov:** Conceptualization (equal); Data curation (equal); Supervision (supporting). **Leonid Merzlikin:** Data curation (supporting); Formal analysis (supporting). **Michael Liverts:** Conceptualization (equal); Methodology (equal). **Maksim Kozlov:** Formal analysis (equal); Software (equal). **Yakov E. Krasik:** Conceptualization (equal); Project administration (lead); Supervision (lead); Writing – original draft (equal); Writing – review & editing (equal).

DATA AVAILABILITY

The data that support the findings of this study are available from the corresponding author upon reasonable request.

REFERENCES

[1]A. W. DeSilva and H.-J. Kunze, Phys. Rev. E **49**, 4448 (1994).
[2]A. W. DeSilva and J. D. Katsouros, Phys. Rev. E **57**, 5945 (1998).
[3]Y. E. Krasik, A. Grinenko, A. Sayapin, S. Efimov, A. Fedotov, V. Z. Gurovich, and V. I. Oreshkin, IEEE Trans. Plasma Sci. **36**, 423 (2008).
[4]J. Stephens, J. Dickens, and A. Neuber, Phys. Rev. E **89**, 053102 (2014).
[5]Y. E. Krasik, S. Efimov, D. Sheftman, and A. Fedotov-Gefen, IEEE Trans. Plasma Sci. **44**, 412 (2016).
[6]V. E. Fortov and I. T. Iakubov, *The Physics of Non-Ideal Plasma* (World Scientific, Singapore, 2000).
[7]R. P. Drake, *High-Energy-Density Physics: Fundamentals, Inertial Fusion, and Experimental Astrophysics* (Springer-Verlag, Berlin/Heidelberg, 2006).
[8]F. Graziani, M. P. Desjarlais, R. Redmer, and S. B. Trickey, *Warm Dense Matter and High Energy Density Physics* (Springer International Publishing, Switzerland, 2014).
[9]J. Larsen, *Foundations of High-Energy-Density Physics: Physical Processes of Matter at Extreme Conditions* (Cambridge University Press, 2017).
[10]S. V. Lebedev, A. Frank, and D. D. Rutov, "Exploring astrophysics-relevant magnetohydrodynamics with pulsed-power laboratory facilities," Rev. Mod. Phys. **91**, 025002 (2019).
[11]A. Grinenko, S. Efimov, A. Fedotov, and Y. E. Krasik, J. Appl. Phys. **100**, 113509 (2006).
[12]S. Efimov, V. T. Gurovich, G. Bazalitski, A. Fedotov, and Y. E. Krasik, J. Appl. Phys. **106**, 073308 (2009).
[13]A. Fedotov-Gefen, S. Efimov, L. Gilburd, G. Bazalitski, V. T. Gurovich, and Y. E. Krasik, Phys. Plasmas **18**, 062701 (2011).
[14]D. Shafer, V. T. Gurovich, D. Yanuka, E. Zvulun, S. Gleizer, G. Toker, and Y. E. Krasik, J. Appl. Phys. **117**, 015901 (2015).
[15]D. Maler, S. Efimov, A. Rososhek, S. N. Bland, and Y. E. Krasik, Phys. Plasmas **28**, 063509 (2021).
[16]D. Maler, M. Kozlov, S. Efimov, and Y. E. Krasik, Phys. Plasmas **29**, 032705 (2022).
[17]A. M. Saunders, C. V. Stan, K. K. Mackay, B. Morgan, J. A. K. Horwitz, S. J. Ali, H. G. Rinderknecht, T. Haxhimali, Y. Ping, F. Najjar, J. Eggert, and H. S. Park, Phys. Rev. Lett. **127**, 155002 (2021).
[18]D. Maler, A. Rososhek, S. Efimov, A. Virozub, and Y. E. Krasik, J. Appl. Phys. **129**, 034901 (2021).
[19]A. Fedotov, D. Sheftman, V. T. Gurovich, S. Efimov, G. Bazilitski, Y. E. Krasik, and V. I. Oreshkin, Phys. Plasmas **15**, 082704 (2008).
[20]A. Fedotov-Gefen, S. Efimov, L. Gilburd, S. Gleizer, G. Bazalitsky, V. T. Gurovich, and Y. E. Krasik, Appl. Phys. Lett. **96**, 221502 (2010).
[21]A. Grinenko, Y. E. Krasik, S. Efimov, A. Fedotov, V. T. Gurovich, and V. I. Oreshkin, Phys. Plasmas **13**, 042701 (2006).
[22]D. Maler, S. Efimov, M. Liverts, S. Theocharous, J. Strucka, Y. Yao, W. Proud, A. Rack, B. Lukic, S. N. Bland, and Y. E. Krasik, Phys. Plasmas **29**, 063502 (2022).
[23]G. Bazalitski, V. T. Gurovich, A. Fedotov-Gefen, S. Efimov, and Y. E. Krasik, Shock Waves **21**, 321 (2011).
[24]S. Lyon and J. Johnson, "SESAME: The Los Alamos National Laboratory Equation of State Database," Report No. LA-UR-92-3407, 1992.
[25]R. H. Cole, *Underwater Explosion* (Princeton University Press, Princeton, New Jersey, 1948).
[26]M. Bystritsky, V. M. Grebenyuk, S. S. Parzhitski, F. M. Pen'kov, V. T. Sidorov, V. A. Stolupin, T. L. Bulgakov, G. A. Mesyats, A. A. Sinebryukhov, and V. A. Sinebryukhov, Laser Part. Beams **18**, 325 (2000).
[27]M. Bystritsky, V. V. Gerasimov, A. R. Krylov, S. S. Parzhitski, F. M. Pen'kov, O. M. Shvyryaev, V. A. Stolupin, G. N. Dudkin, B. A. Nechaev, V. M. Padalko, *et al.*, Yad. Fiz. **66**, 1731 (2003) [Phys. At. Nucl. **66**, 1683 (2003)].